

Generalized plasma dispersion function: One-solve-all treatment, visualizations, and application to Landau damping

Cite as: Phys. Plasmas **20**, 092125 (2013); <https://doi.org/10.1063/1.4822332>

Submitted: 16 July 2013 • Accepted: 02 September 2013 • Published Online: 30 September 2013

Hua-Sheng Xie (谢华生)



View Online



Export Citation



CrossMark

ARTICLES YOU MAY BE INTERESTED IN

[The modified plasma dispersion function](#)

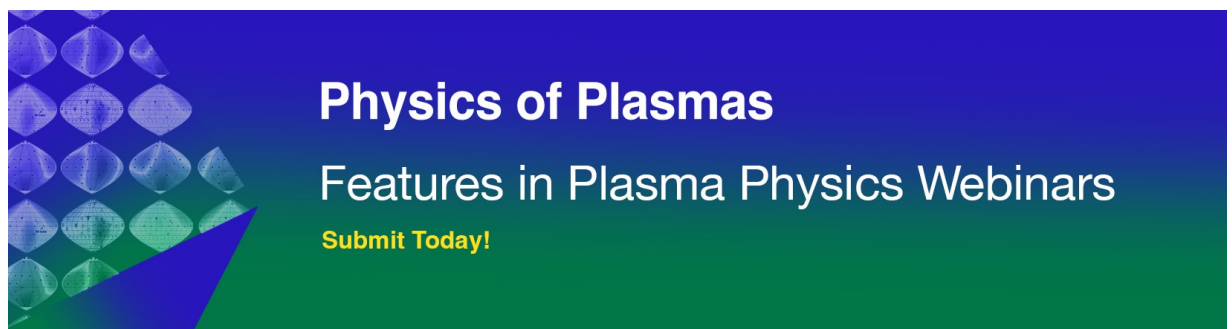
Physics of Fluids B: Plasma Physics **3**, 1835 (1991); <https://doi.org/10.1063/1.859653>

[The incomplete plasma dispersion function: Properties and application to waves in bounded plasmas](#)

Physics of Plasmas **20**, 012118 (2013); <https://doi.org/10.1063/1.4789387>

[A new formulation and simplified derivation of the dispersion function for a plasma with a kappa velocity distribution](#)

Physics of Plasmas **16**, 072113 (2009); <https://doi.org/10.1063/1.3179807>



Generalized plasma dispersion function: One-solve-all treatment, visualizations, and application to Landau damping

Hua-Sheng Xie (谢华生)^{a)}

Institute for Fusion Theory and Simulation, Zhejiang University, Hangzhou 310027, People's Republic of China

(Received 16 July 2013; accepted 2 September 2013; published online 30 September 2013)

A unified, fast, and effective approach is developed for numerical calculation of the well-known plasma dispersion function with extensions from Maxwellian distribution to almost arbitrary distribution functions, such as the δ , flat top, triangular, κ or Lorentzian, slowing down, and incomplete Maxwellian distributions. The singularity and analytic continuation problems are also solved generally. Given that the usual conclusion $\gamma \propto \partial f_0 / \partial v$ is only a rough approximation when discussing the distribution function effects on Landau damping, this approach provides a useful tool for rigorous calculations of the linear wave and instability properties of plasma for general distribution functions. The results are also verified via a linear initial value simulation approach. Intuitive visualizations of the generalized plasma dispersion function are also provided.

© 2013 AIP Publishing LLC. [<http://dx.doi.org/10.1063/1.4822332>]

I. INTRODUCTION

In a one-dimensional, one-species, non-relativistic electrostatic plasma system, the Langmuir wave dispersion relation is¹

$$D(k, \omega) = 1 - \frac{\omega_p^2}{k^2} \int_C \frac{\partial f_0 / \partial v}{v - \omega/k} dv = 0, \quad (1)$$

where k is the wave vector, $\omega = \omega_r + i\gamma$ is the frequency, $\omega_p = \sqrt{4\pi n_0 q^2 / m}$ is the plasma frequency, and C is the Landau integral contour.

For Maxwellian distribution $f_0 = F_M$, with

$$F_M(v) = \frac{1}{\sqrt{\pi} v_t} e^{-\frac{v^2}{v_t^2}}, \quad (2)$$

the well-known plasma dispersion function (PDF),

$$Z_M(\zeta) = \frac{1}{\sqrt{\pi}} \int_{-\infty}^{\infty} \frac{e^{-z^2}}{z - \zeta} dz, \quad \Im(\zeta) > 0, \quad (3)$$

with analytic continuation to $\Im(\zeta) \leq 0$, is defined by Fried and Conte,² where $\zeta = \omega / (kv_t)$ and $z = v/v_t$. Hence, Eq. (1) is rewritten to

$$D(k, \omega) = 1 - \frac{1}{(k\lambda_D)^2} \frac{1}{2} Z'_M(\zeta) = 0, \quad (4)$$

with also

$$Z'_M(\zeta) = -2[1 + \zeta Z_M(\zeta)], \quad (5)$$

where $\lambda_D = \sqrt{T/m} / \omega_p$ and $v_t = \sqrt{2T/m}$. A $\sqrt{2}$ difference in the normalizations between v_t and T should be noted.

Analytic properties and numerical approaches for the usual PDF (Eq. (3)), which is similarly related to complex error function, Faddeeva function, or Dawson integral, have been extensively studied since Fried and Conte.² Good $Z_M(\zeta)$ function numerical schemes for practical application can also be easily found. However, in studying other distribution functions, it should be treated separately. The singularity in real line and analytic continuation to $\Im(\zeta) \leq 0$ usually requires careful treatment, otherwise it would be confusing and would yield incorrect results.

A family of distributions, i.e., κ distributions or generalized Lorentzian distributions³

$$F_\kappa = A_\kappa \left[1 + \frac{1}{\kappa} \frac{v^2}{v_t^2} \right]^{-\kappa}, \quad (6)$$

with the normalization constant

$$A_\kappa = \frac{1}{v_t} \frac{\Gamma(\kappa)}{\Gamma(\kappa - 1/2)} \frac{1}{\sqrt{\pi\kappa}}, \quad (7)$$

are very useful for space and astrophysical plasma and have been studied intensively since Summers and Thorne,⁴ where Γ is the Euler gamma function. Recently, Baalrud⁵ also investigated a semi-infinite integral for Maxwellian distribution, called the incomplete PDF.

Each author uses his or her own technique to treat the Landau contour. For instance, Baalrud⁵ treated the incomplete PDF via direct numerical integral and continued fraction expansion, whereas Hellberg and Mace⁶ treated the κ distribution using Gauss hypergeometric function.

The generalized plasma dispersion function (GPDF) can be defined as

$$Z(\zeta) = Z(\zeta, F) = \int_C \frac{F}{z - \zeta} dz, \quad (8)$$

and its derivative,

^{a)}Electronic mail: huashengxie@gmail.com

$$Z_p(\zeta) = \int_C \frac{\partial F / \partial z}{z - \zeta} dz = Z'(\zeta, F), \quad (9)$$

with the original PDF as a special case when $F = e^{-z^2}/\sqrt{\pi}$. Developing systematic methods to treat arbitrary physical reasonable distribution functions (e.g., $f \geq 0$, $\int f dv < \infty$) in one scheme, i.e., one-solve-all, is advantageous. For instance, several typical distribution functions are shown in Fig. 1.

In this study, we investigate the analytical properties (particularly the singularity and analytic continuation problems) and develop a general numerical scheme for GPDP, i.e., for almost arbitrary input function F .

This problem was also discussed by Robinson,⁷ who used the linear combination of orthogonal functions. Three sets of orthogonal functions, Hermite, Legendre, and Chebyshev polynomials were discussed. Robinson's method is very similar to our treatment in this study. However, he has neither given systematic results of the analytic continuation nor developed a one-solve-all scheme for practical application.

Our approach, which is discussed in Sec. II, is based on Hilbert transform (HT) and fast Fourier transform (FFT). After solving GPDP generally, we show several visualizations of GPDP in Sec. III. The distribution function effects on Landau damping are revisited in Sec. IV, and a summary and discussion are given in Sec. V.

II. ONE-SOLVE-ALL SCHEME FOR GENERALIZED PLASMA DISPERSION FUNCTION

A. Hilbert transform and analytic continuation

HT is defined as

$$g(z) = H(f(z)) = \frac{1}{\pi} \int_{-\infty}^{\infty} \frac{f(z')}{z' - z} dz', \quad (10)$$

which can also be viewed as a convolution,

$$g(z) = \frac{1}{\pi z} * f(z), \quad (11)$$

or the inverse,

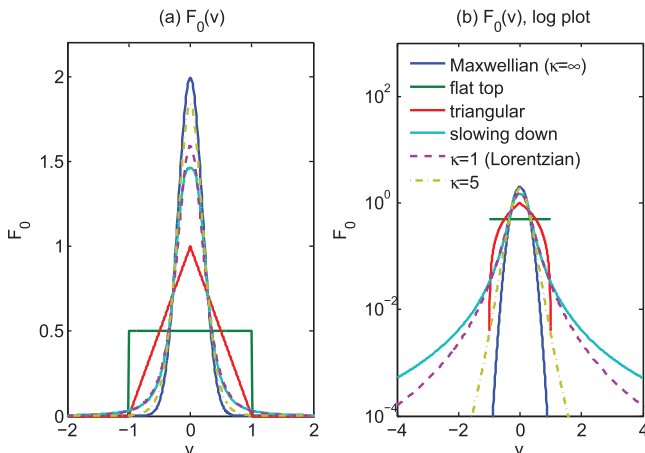


FIG. 1. Typical distribution functions.

$$f(z) = -\frac{1}{\pi z} * g(z), \quad (12)$$

where $f(z)$ and $g(z)$ are called a Hilbert pair. HT usually represents a 90° phase shift of input function.

Some useful properties include

1. $H(c_1 f_1(z) + c_2 f_2(z)) = c_1 g_1(z) + c_2 g_2(z)$,
2. $H(H(f(z))) = -f(z)$,
3. $H(f(z+a)) = g(z+a)$,
4. $H(f(az)) = \text{sgn}(a)g(az)$,
5. $H\left(\frac{d^n f(z)}{dz^n}\right) = \frac{d^n g(z)}{dz^n}$,
6. $f(z) + ig(z)$ is an analytical function.

A good scheme for numerically calculating HT in real line is provided by Weideman.⁸ Two other numerical methods are, using Eq. (10), i.e.,

$$g(z) \simeq \frac{2}{\pi} \sum_{n=-\infty}^{\infty} \frac{f(z + (2n+1)h)}{2n+1}, \quad (13)$$

where h is the step size, or using Eq. (11), i.e.,

$$g(z) = \text{ift} \left[\text{ft} \left(\frac{1}{\pi z} \right) \cdot \text{ft}(f(z)) \right], \quad (14)$$

where $\text{ft}()$ and $\text{ift}()$ denote the Fourier transform and its inverse.

The methods in Weideman's 1995 paper⁸ or via Eqs. (13) and (14) are mainly for calculating integral principal value (PV) in real line.

In fact, the definition of Eq. (10) is not a single function. For simplification, we require $f(z)$ be an entire function that is integrable in the range of $-\infty$ to $+\infty$. The plasma dispersion function is defined for $\Im(z) > 0$, and thus, should be extended to $\Im(z) \leq 0$, which is¹⁰

$$g^+(z) = \begin{cases} \frac{1}{\pi} \int_{-\infty}^{\infty} \frac{f(z')}{z' - z} dz', & \Im(z) > 0, \\ \frac{1}{\pi} \text{PV} \int_{-\infty}^{\infty} \frac{f(z')}{z' - z} dz' + if(z), & \Im(z) = 0, \\ \frac{1}{\pi} \int_{-\infty}^{\infty} \frac{f(z')}{z' - z} dz' + 2if(z), & \Im(z) < 0. \end{cases} \quad (15)$$

For instance, the HT of Lorentzian distribution $f(z) = \frac{a}{\pi z^2 + a^2}$ is

$$g(z) = \begin{cases} -\frac{1}{\pi} \frac{1}{(z+ia)}, & \Im(z) > 0, \\ -\frac{z}{(z^2 + a^2)}, & \Im(z) = 0, \\ -\frac{1}{\pi} \frac{1}{(z-ia)}, & \Im(z) < 0, \end{cases} \quad (16)$$

whereas

$$g^+(z) = -\frac{1}{\pi(z+ia)}, \quad (17)$$

which is consistent with Eq. (15).

$g^-(z)$ can be defined in a similar manner if we want to extend a function from lower half plane to the entire complex plane.

Weideman⁹ also provided a method to calculate $g^+(z)$ of the HT of Gaussian function in upper half plane, which is related to PDF $Z_M(\zeta)$.

B. One-solve-all approach

A comparison of Eqs. (8) and (9) with Eq. (15) indicates $Z = \pi g^+$ and $Z_p = \pi g^{'+}$ with $F = f$ and $F' = f'$. Thus, GPDF is merely a HT of distribution function and shares the same properties of HT as listed in Sec. II A.

Jones *et al.*¹⁰ also discussed the contour integral problem of GPDF and used transformation $z = \tan(t)$ to map the integral of $z \in (-\infty, \infty)$ to $t \in (-\pi, \pi)$. This method is merely an alteration of Eq. (13) and requires other tricks to avoid singularity. Moreover, the method is time consuming and not suitable for high accuracy calculation as the discrete step should be very small to avoid divergence. Another direct numerical integral result is shown by Guio *et al.*¹¹ with typical errors of 10^{-4} .

In this paper, we use Eq. (15) to extend Weideman's approach^{8,9} to the entire complex plane, where the orthogonal functions is $e^{i\theta}$, which can be evaluated very rapidly by FFT, instead of the Hermite, Legendre, and Chebyshev polynomials used by Robinson.⁷

The key steps are summarized as follows:

Assuming an expansion,

$$[W(v)]^{-1}F(v) = \sum_{n=-\infty}^{\infty} a_n \rho_n(v), \quad v \in \mathcal{R}, \quad (18)$$

where $\{\rho_n(v)\}$ is an orthogonal basis set with weight function $W(v)$, i.e.,

$$\int_{-\infty}^{\infty} W(v) \rho_n(v) \rho_m^*(v) dv = A \delta_{m,n}, \quad (19)$$

where the asterisk denotes complex conjugation and $\delta_{m,n}$ is the Kronecker delta. The coefficients are

$$a_n = \frac{1}{A} \int_{-\infty}^{\infty} F(v) \rho_n^*(v) dv. \quad (20)$$

Then,

$$\frac{F(v)}{v-z} = \sum_{n=-\infty}^{\infty} a_n \left[W(v) \frac{\rho_n(v)}{v-z} \right]. \quad (21)$$

For the upper half plane, we use weight function $W(v) = 1/(L^2 + v^2)$ (Ref. 9) and basis functions,

$$\rho_n(v) = \frac{(L + iv)^n}{(L - iv)^n}, \quad (22)$$

which is a Fourier form because $e^{i\theta} = (L + iv)/(L - iv)$ with $v = L \tan(\theta/2)$ and $dv/d\theta = (L^2 + v^2)/(2L)$, then a_n can be evaluated using FFT and we can obtain $A = \pi/L$ using $\int_{-\pi}^{\pi} e^{in\theta} e^{-im\theta} d\theta = 2\pi \delta_{m,n}$.

Using residues, for $\Im(\zeta) > 0$, we find the integrals

$$\int_{-\infty}^{\infty} \frac{W(v) (L + iv)^n}{v - z (L - iv)^n} dv = \begin{cases} \frac{i\pi}{L} \frac{1}{(L - iz)}, & n = 0, \\ \frac{2i\pi}{L^2 + z^2} \frac{(L + iz)^n}{(L - iz)^n}, & n > 0, \\ 0, & n < 0. \end{cases} \quad (23)$$

We obtain

$$g^+(z) = \frac{2i}{L^2 + z^2} \sum_{n=1}^{\infty} a_n \left(\frac{L + iz}{L - iz} \right)^n + \frac{ia_0}{L(L - iz)}, \quad \Im(z) > 0. \quad (24)$$

For the lower half plane, $\Im(\zeta) < 0$, we use $F(z) = [F(z^*)]^*$ and obtain

$$Z(\zeta) = [Z(\zeta^*)]^* + 2i\pi f(\zeta), \quad \Im(\zeta) < 0. \quad (25)$$

For real line, $\Im(\zeta) = 0$, we use $W(v) = 1$ and $\rho_n(v) = (L + iv)^n / (L - iv)^{n+1}$,⁸ and obtain

$$g^+(z) = \sum_{n=-\infty}^{\infty} i \operatorname{sgn}(n) a_n \rho_n(z) + i f(z), \quad (26a)$$

$$= \sum_{n=0}^{\infty} 2i a_n \rho_n(z), \quad \Im(z) = 0. \quad (26b)$$

We have avoided the singularity on real line by treating the integrals of the basis functions analytically.

A completed scheme¹⁶ is provided through the combination of Eqs. (24)–(26), which can support an almost arbitrary smooth distribution function $F(v)$ and $F_p(v) = \partial F / \partial v$ as input function.

In numerical calculation, we truncate the summation at a finite point $n = N$. In the practical test for Gaussian input function with $N = 32$, the program delivers twelve significant decimal digits,⁹ where L is an optimal parameter and is set to $2^{-1/4} N^{1/2}$ as default.

Another good feature of this approach is that the coefficients a_n need only be calculated once for all z , making the scheme even faster.

Moreover, an unexpected but interesting feature is that, the input function in the L.H.S. of Eq. (18) is not necessarily a smooth function. The R.H.S. of Eq. (18) can transform the real function $F(v)$ in real line to a smooth analytic complex function in whole complex plane with truncation. This feature can help us calculate several (note: not all) non-smooth input functions directly, such as flat top, incomplete Maxwellian, and slowing down. The validity of this approximation will be verified in Sec. III.

III. VISUALIZATIONS OF GENERALIZED PLASMA DISPERSION FUNCTION

A. Maxwellian distribution

First, we compare the results of the usual PDF with Maxwellian distribution as input function.

Fig. 2 shows a comparison of our scheme (using $N = 32$) with exact $Z(\zeta)$ function via complex error function in

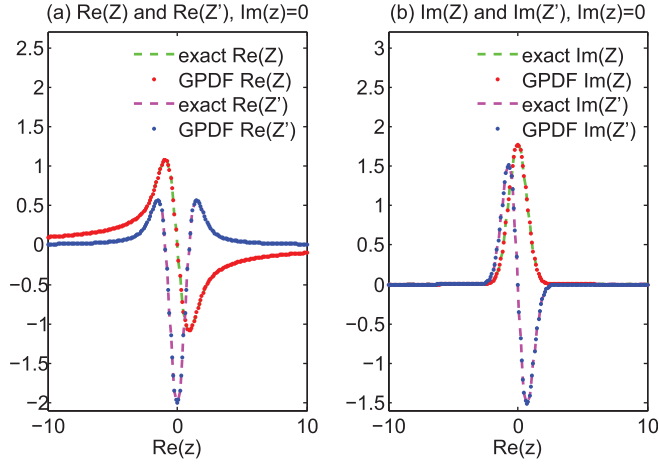


FIG. 2. Comparison of our scheme for GPDF with exact $Z(\zeta)$ function via complex error function in standard numerical library on real axis.

standard numerical library on real axis. We find the errors to be around 10^{-12} (not shown in the figure), e.g., $Z(1) = -1.076159013825734 + 0.652049332173291i$ in our scheme and $Z(1) = -1.076159013825537 + 0.652049332173292i$ via standard library.

Fig. 3 shows the 2D visualizations of $Z(\zeta)$ and $Z'(\zeta)$ produced by our scheme, which shows that the functions are indeed analytically smooth. If we exclude the step for analytic continuation, we will find a jump at real line $\Im(z) = 0$ (not shown here).

B. κ distribution

With $F = \frac{1}{\pi(v^2+1)}$ as input function, a result is shown in Fig. 4, where we can find a singularity at $z = -i$, which is consistent with analytical result Eq. (17).

However, another artificial singular point at $z = i$ [see panel (a)] can be found, where the code yields NaN . The two first-order singular points $v - ia = 0$ and $v - z = 0$ transformed into one second-order singular point $(v - ia)^2 = 0$ when $z = ia$ for Lorentzian input function. An extra approximation $Z(\zeta_0) \simeq Z(\zeta_0 + \epsilon)$ in the code is used to treat this kind of singular point, with ζ_0 as the artificial singular point and ϵ be a small number, e.g., 10^{-10} . After the extra treatment, we find GPDF yields exactly the same values as $\pi \times$ Eq. (17) in all computation grids (not shown here) with controllable small errors.

After fixing this problem, a result is shown in Fig. 5 for $\kappa = 5$, $v_i = 1$.

To keep $\kappa = 1$ the usual Lorentzian distribution, the definition of κ -distribution in Eq. (6) slightly differs from the usual one⁴ but is close to the one by Valentini and D'Agosta.³

C. δ distributions

The scheme described in Sec. II cannot support several non-standard distribution functions directly, particularly, δ distribution, which has been widely used for modeling cold plasma. We treat it separately in the code, via analytical expression.

For δ -distribution $F_\delta = \delta(z - z_d)$,

$$Z(\zeta) = -\frac{1}{\zeta - z_d}, \quad (27a)$$

$$Z_p(\zeta) = \frac{1}{(\zeta - z_d)^2}, \quad (27b)$$

which can also be obtained from Eq. (17) using the limit $a \rightarrow 0$ because $\delta(v) = \lim_{a \rightarrow 0} \frac{1}{\pi} \frac{a}{v^2 + a^2}$. The result is shown in Fig. 6.

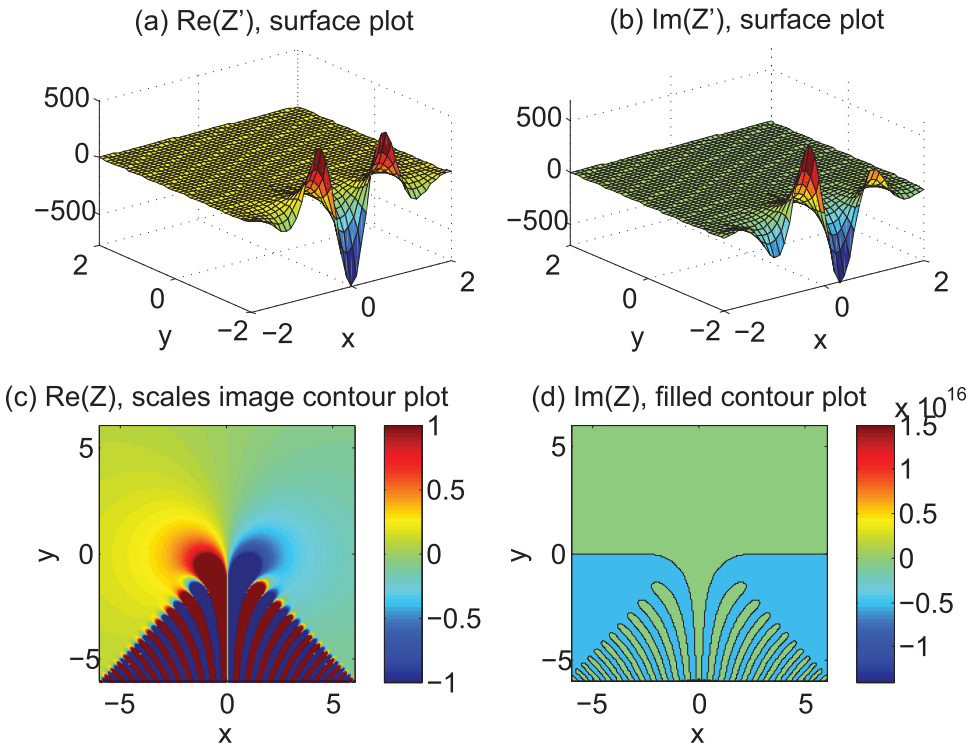


FIG. 3. Visualization of $Z(\zeta)$ and $Z'(\zeta)$ with Maxwellian input function.

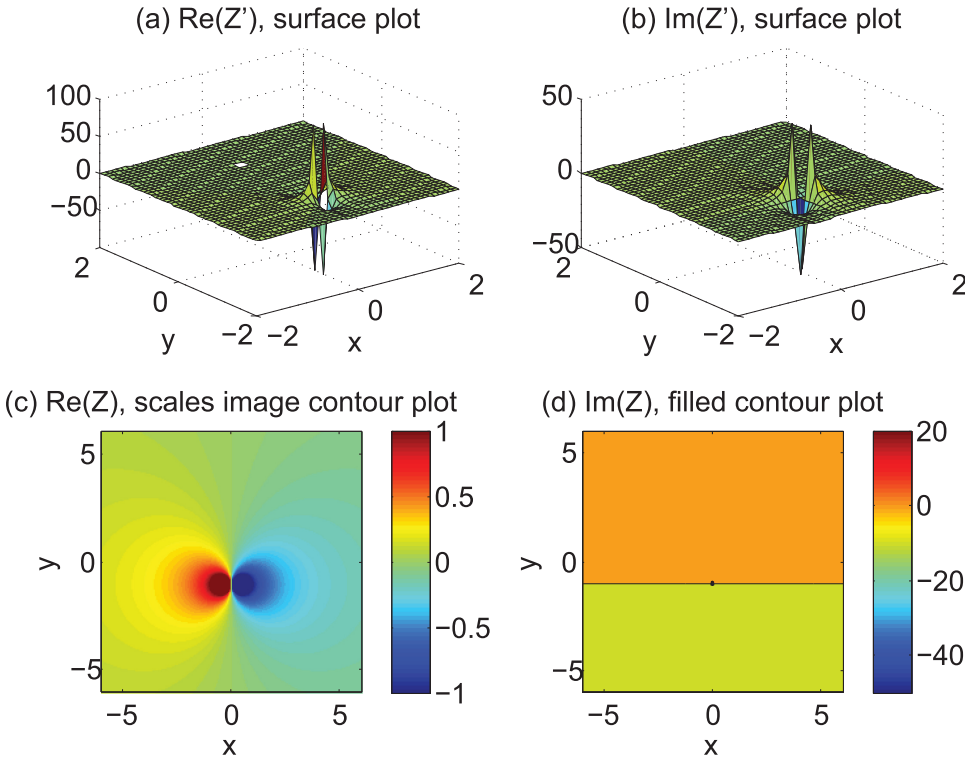


FIG. 4. Visualization of $Z(\zeta)$ and $Z'(\zeta)$ with input function $F = \frac{1}{\pi(v^2+1)}$, where artificial singular point $N\alpha N$ at $\zeta = i$ is kept.

D. Incomplete Maxwellian distributions

The input function is

$$F_{\text{IM}}(v) = H(v - \nu) \frac{1}{\sqrt{\pi}} e^{-v^2}, \quad (28)$$

which has been investigated comprehensively by Baalrud,⁵ where H is the Heaviside step function.

As previously mentioned, the numerical scheme cannot treat the δ function directly. For Z' , an extra correction term

should be added, i.e., $Z'_{\text{IM}}(\zeta) = Z'_{\text{IM0}}(\zeta) - \frac{1}{\sqrt{\pi}} e^{-\nu^2} / (\zeta - \nu)$, where Z'_{IM0} is the result without correction.

Fig. 7 shows the results of $Z_{\text{IM}}(\zeta)$ and $Z'_{\text{IM0}}(\zeta)$ calculated from our GPDF scheme, with $\nu = 1$, $N = 1024$, and $L = 10$. Fig. 7(a) is in favor of Fig. 3(b) by Baalrud,⁵ which was calculated from a direct numerical integral. Our one-solve-all scheme can solve the same problem at least ten times faster than the direct numerical integral usually with the same accuracy.

A slight error can be found around the real line when N is small, say $N = 64$, which arises from the error of Fourier

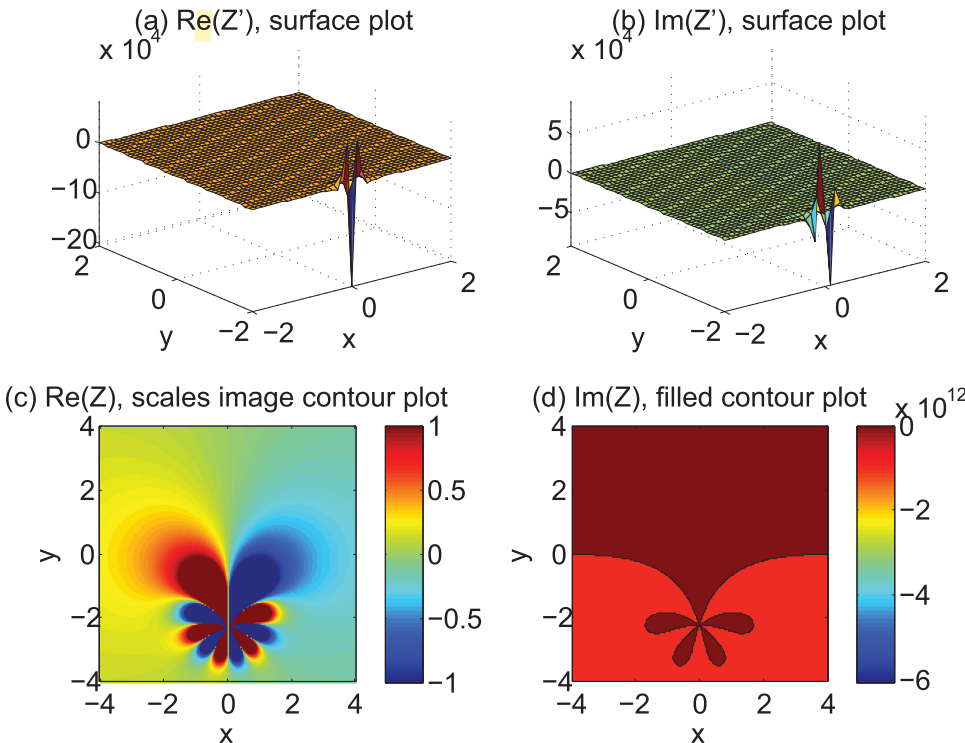


FIG. 5. Visualization of $Z(\zeta)$ and $Z'(\zeta)$ with input function $F_{\kappa=5}$.

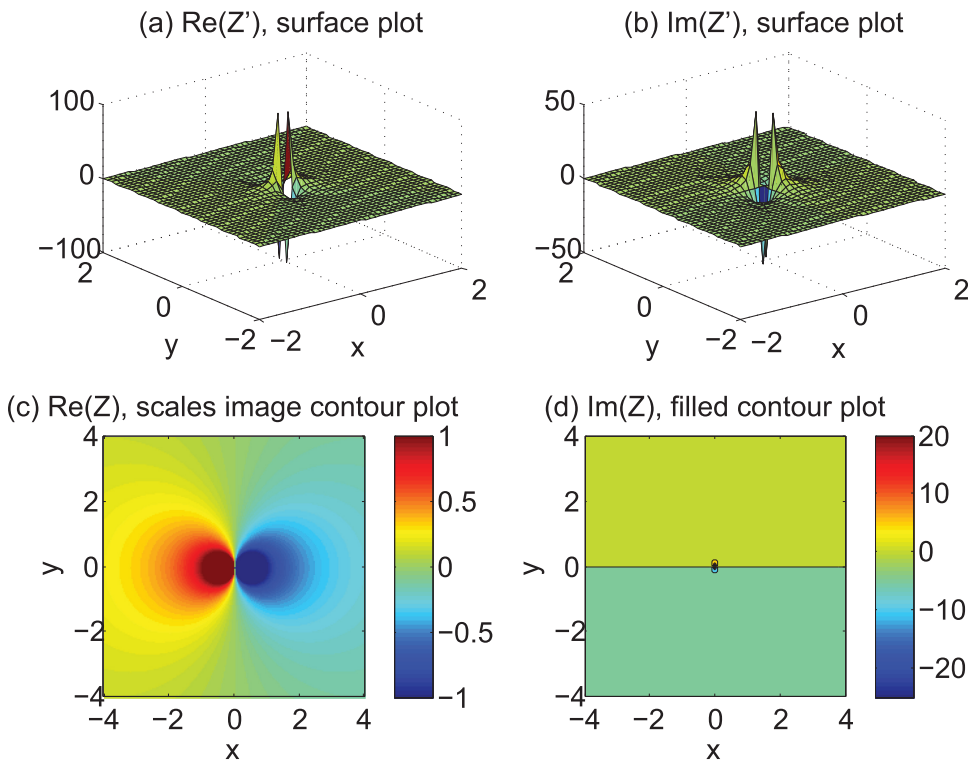


FIG. 6. Visualizations of $Z(\zeta)$ with input function F_δ and parameters $z_d = 0$.

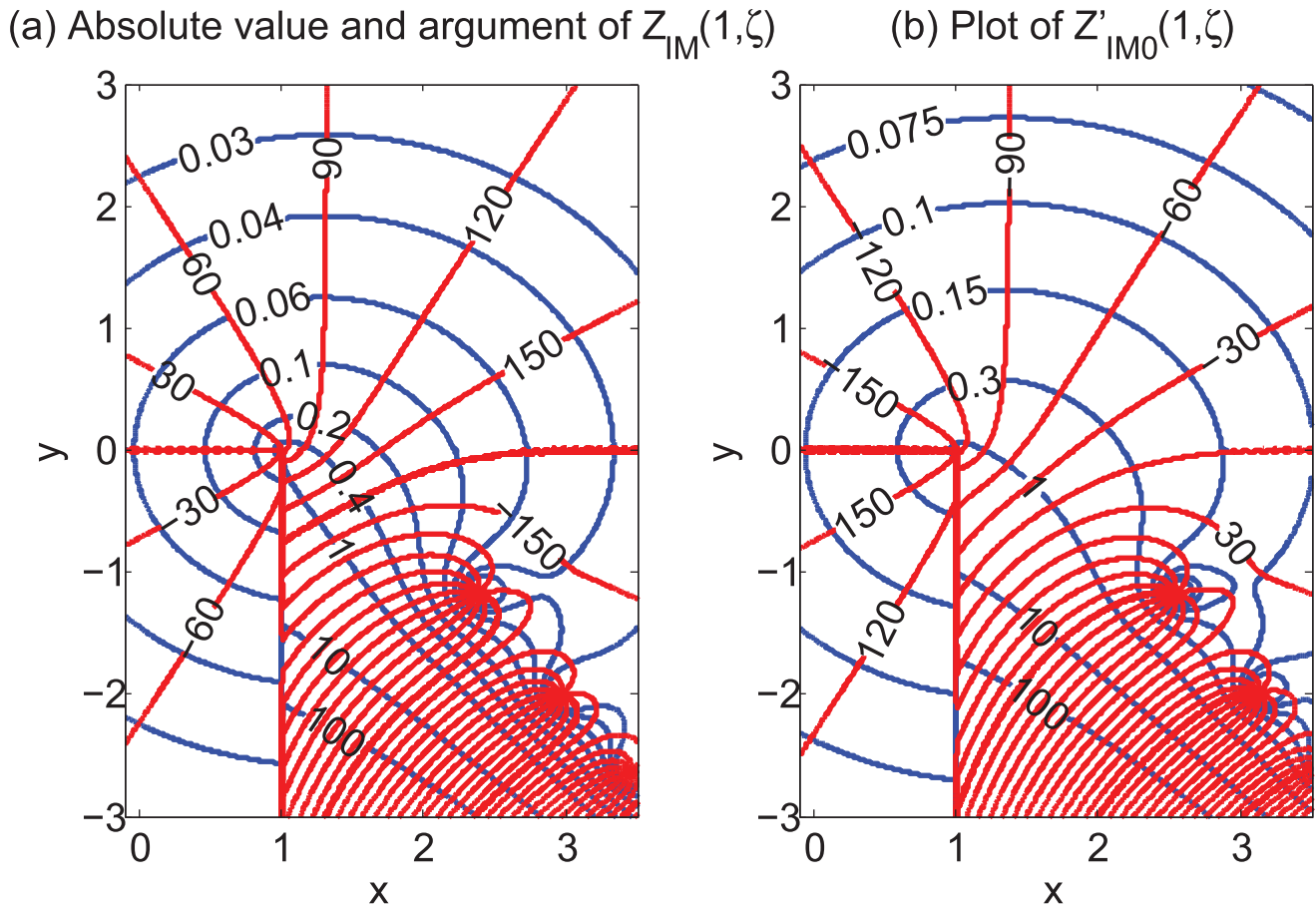


FIG. 7. Visualization of $Z_{\text{IM}}(\zeta)$ and $Z'_{\text{IM0}}(\zeta)$ with input function (28), where the absolute value and argument are calculated using $Z = |Z|e^{i\theta}$.

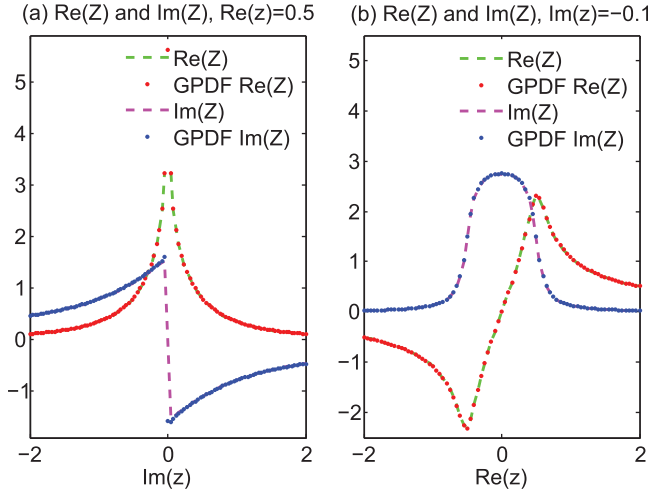


FIG. 8. Comparison of GPDF results and analytical results for $Z(\zeta)$ with input function F_{Rect} and parameters $z_a = -0.5$ and $z_b = 0.5$.

expansion around the sharp step place (Gibbs phenomenon) that requires a large N to overcome.

E. Flat top distribution

For flat top distribution $F_{\text{Rect}} = \frac{H(z-z_a) - H(z-z_b)}{z_b - z_a}$,

$$Z(\zeta) = \frac{1}{z_b - z_a} [\ln(\zeta - z_b) - \ln(\zeta - z_a)], \quad (29a)$$

$$Z_p(\zeta) = \frac{1}{z_b - z_a} \left[\frac{1}{\zeta - z_b} - \frac{1}{\zeta - z_a} \right]. \quad (29b)$$

GPDF results and analytical results are compared in Fig. 8. This benchmark indicates that our treatment for GPDF is indeed suitable for both smooth and non-smooth input function. However, to keep the result exactly the same as Eq. (29) at

range $z_a \leq \zeta \leq z_b$ for lower half plane [$\Im(\zeta) < 0$], the analytic continuation term $2if(z)$ is set to zero, instead of $2i/(z_b - z_a)$.

For Z'_{Rect} , we need also an extra treatment because of the δ function.

F. Triangular distribution

The distribution function is

$$F_{\text{Tri}} = \frac{H(z - z_a) - H(z - z_b)}{(z_b - z_a)} \frac{2}{z_c - z_a} (z - z_a) - \frac{H(z - z_b) - H(z - z_c)}{(z_c - z_b)} \frac{2}{z_c - z_a} (z - z_c), \quad (30)$$

and corresponding $Z(\zeta)$ is shown in Fig. 9.

The analytic continuation term $2if(z)$ for lower half plane [$\Im(\zeta) < 0$] is set to zero. Comparing root finding results and simulation results of Langmuir wave using the methods discussed in Sec. IV, we find that the solutions are the same (not shown here) for both cases, i.e., setting the term to zero or non-zero, and agreed with the simulations.

G. Slowing down distributions

The distribution function is very common in fusion plasma, such as tokamak, for fast particles,

$$F_{\text{SD}} = \frac{3\sqrt{3}v_t^2}{4\pi} \frac{1}{|v|^3 + v_t^3} H(v_c - |v|). \quad (31)$$

A result is shown in Fig. 10.

One should note that the absolute value of v in F could cause problems in the complex plane, as $|\Re(v) + i\Im(v)| = \sqrt{\Re(v)^2 + \Im(v)^2} \neq |\Re(v)| + i\Im(v)$. We use $H(v)$ to rewrite $|v|$ in the code, where $H(\Re(v) + i\Im(v))$

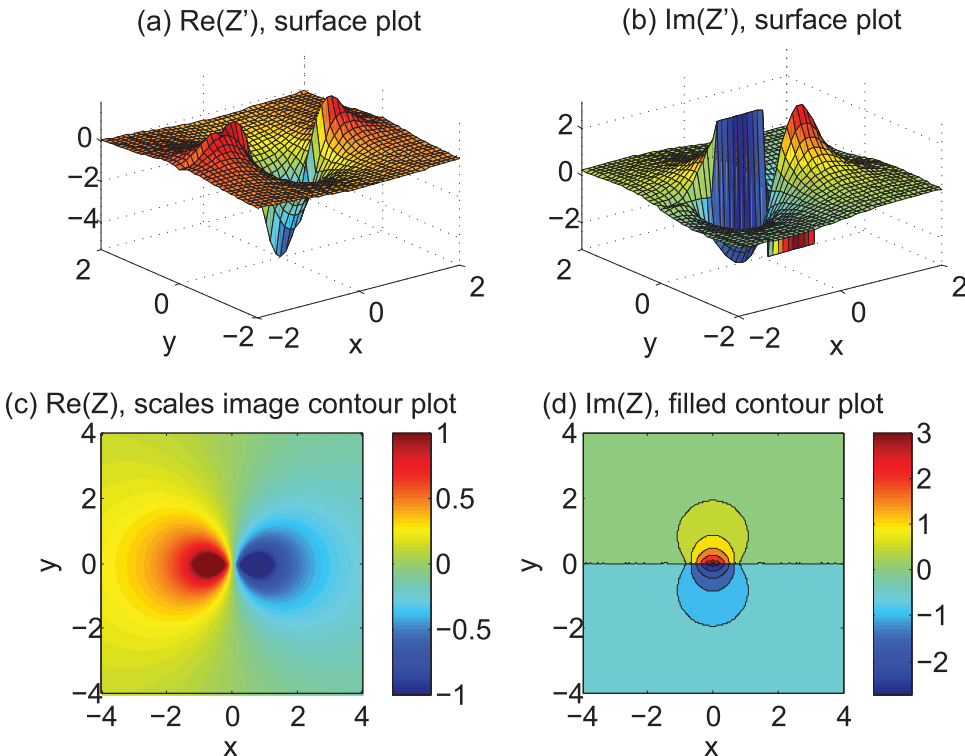


FIG. 9. Visualization of $Z(\zeta)$ and $Z'(\zeta)$ with input function F_{Tri} and parameters $z_a = -1.0$, $z_b = 0$ and $z_c = 1$.

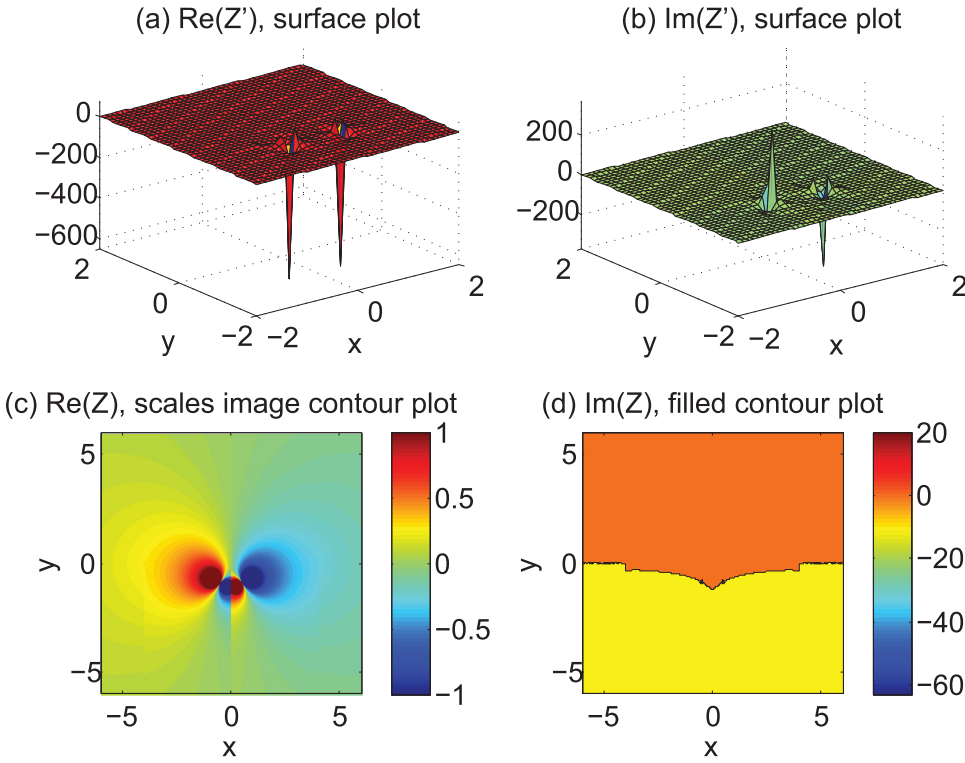


FIG. 10. Visualization of $Z(\zeta)$ and $Z'(\zeta)$ with input function F_{SD} for $v_t = 1$ and $v_c = 4$.

$= H(\Re(v))[\Re(v) + i\Im(v)]$. Hence, we can still use $if(z)$ directly for the analytic continuation term to reduce numerical errors, instead of using the expansion expression $\sum a_n \rho_n$.

H. Other distributions

The GPDF has several good features such as for the bump-on-tail problem, when using usual PDF, the core plasma and beam plasma should be treated separately. We can treat it using one input function directly when using

GPDF. A result is shown in Fig. 11 for $F = 0.9e^{-v^2}/\sqrt{\pi} + 0.1e^{-(v-2)^2}/\sqrt{\pi}$. A comparison with Fig. 3 shows the beam tail affects $Z(\zeta)$ apparently, particularly at the place around $\Re(\zeta) = v_d = 2$.

I. Short summary

The one-solve-all scheme has been shown to be effective. However, to treat non-smooth/analytical input functions, extra corrections should be noted. For non-smooth flat

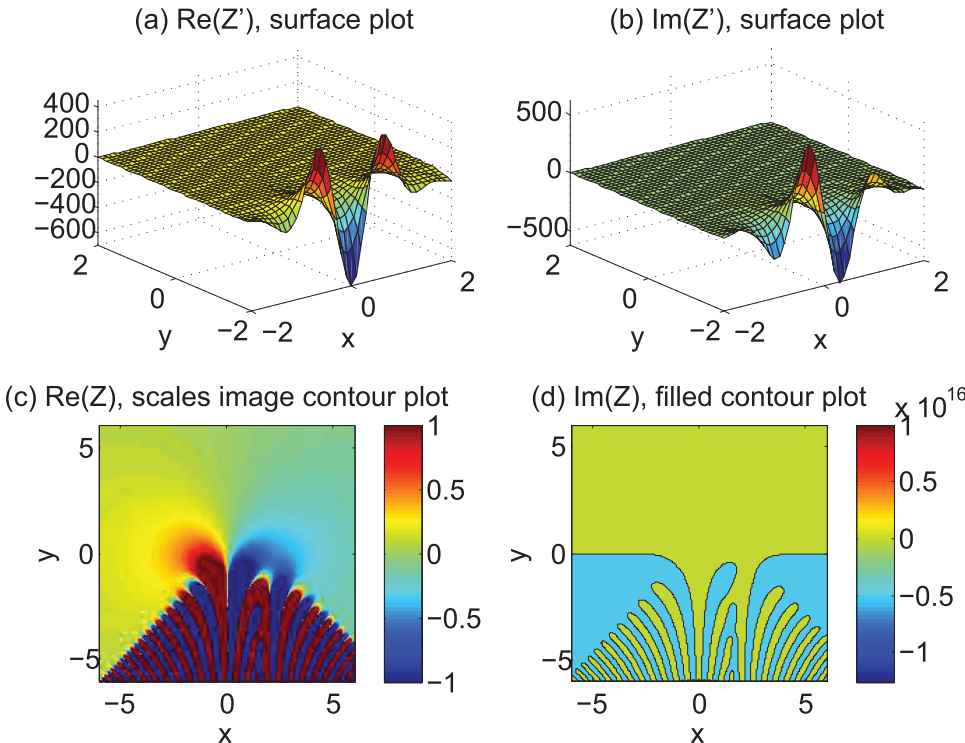


FIG. 11. Visualization of $Z(\zeta)$ and $Z'(\zeta)$ with bump-on-tail input function.

top and triangular distributions, the method of determining the analytic continuation requires further investigation, because it cannot be distinguished by Langmuir wave simulation.

From the visualizations of $Z(\zeta)$ and $Z'(\zeta)$ for different types of input functions, the quantitative value, shape, or topology of Z and Z' vary considerably, which will then bring different kinetic effects, e.g., Landau damping rate.

IV. DISTRIBUTION FUNCTION EFFECTS ON LANDAU DAMPING

A. Benchmark GPDF using initial value scheme

For the initial value scheme, the starting equations are the normalized linear Vlasov-Poisson equations

$$\begin{cases} \partial_t \delta f = -ikv\delta f + \delta E \partial_v f_0, \\ ik\delta E = -\int \delta f dv. \end{cases} \quad (32)$$

We usually set $\lambda_D = 1$, then $v_t = \sqrt{2}$ in the initial distribution function f_0 , e.g., $f_0 = \exp(-v^2/2)/\sqrt{2\pi}$ for Maxwellian.

Equation (32) can be solved as an initial value problem (IVP), e.g., using a 4th-order Runge-Kutta scheme, which should produce the exact linear Landau damping when the Case-Van Kampen mode and numerical errors are ignored.¹² This simulation approach can be a simple and/or final benchmark for GPDF. Disagreements would mean the GPDF has been treated incorrectly. However, the IVP approach is not general, because of the numerical errors from discrete of v and t , especially when the phase velocity $v_p = \omega/k$ or damping rate are large. A similar but more complicated IVP approach is used by Valentini and D'Agosta.³ Particle (e.g., particle-in-cell) simulation can also be used, which was also used by Godfrey *et al.*¹⁴ Particle method can also easily support non-smooth distribution, but is limited by the noise resulting in unfavorable errors. Thus, this technique is not accurate when compared with the above continuum method.

Landau damping of Maxwellian distribution using this continuum IVP approach is verified in a previous work.¹²

We check the Lorentzian distribution to show that our scheme for GPDF with non-Maxwellian distributions is also correct. Fig. 12 shows the comparison of Lorentzian distribution Landau damping using IVP scheme and GPDF for

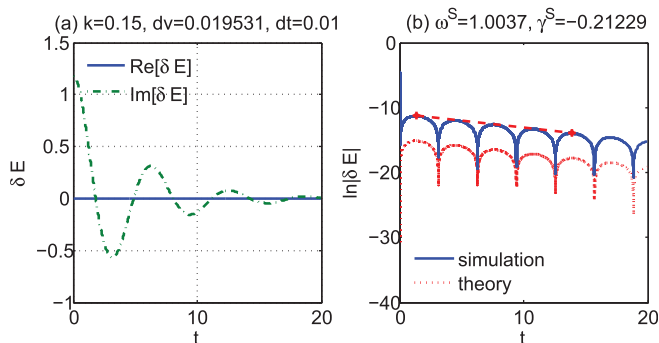


FIG. 12. Benchmark GPDF using initial value simulation for Lorentzian distribution function. The result of root finding for this case is $\omega = 1.0000 - 0.2121i$.

$k=0.15$ and $v_t = \sqrt{2}$. We find that the simulation and numerical/analytical solutions match very well for both real frequency and damping rate, i.e., $\omega = 1.00 - 0.212i$.

Another possible numerical approach for Eq. (32) is to treat it as an eigenvalue problem. However, the (Landau) damping normal mode is not eigenmode in this system, as discussed by numerous authors (see e.g., Ref. 12 and references in). Thus, this approach does not work.

Notably, for GPDF, Eq. (5) would no longer be hold. Thus, Z_p should be used for root finding instead of Z to Eq. (4) or (1).

B. Effects of discontinuity point

The δ function can be modeled as cold plasma, which provides the dispersion relation $(\omega - kv_d)^2 = \omega_p^2$. For discontinuity point such as the cases we meet in incomplete Maxwellian or flat top distributions, Eq. (29) can be used to solve the flat top case easily, which gives $(\omega - kv_d)^2 = \omega_p^2 + k^2 v_t^2$, where $v_t = (z_b - z_a)/2$ and $v_d = (z_b + z_a)/2$. The dispersion relation solutions of δ and flat top distributions are verified by PIC (particle-in-cell) simulation (not shown here). For instance, for flat top distribution $v_t = 1.0$, $v_d = 0$, $k = 1.0$, we obtain $\omega = 1.414$, whereas PIC simulation yields $\omega_r \simeq 1.40$. For the continuum IVP simulation of discontinuity point, we use the approximation $\partial f_0 / \partial v = [f_0(v_0^+) - f_0(v_0^-)] / \Delta v$, where Δv is the velocity space grid size. In a practical test, the simulation also yields the same result, but is more accurate and has lower noise than PIC simulation. Thus, we use continuum IVP to verify GPDF results.

For incomplete Maxwellian distribution, we can compare the dispersion relation solutions of $Z'_{IM}(\zeta)$ and $Z'_{IM0}(\zeta)$ to investigate the effects of discontinuity point.

The results are shown in Fig. 13, with $\nu = -0.1v_t$ and $v_t = \sqrt{2}$. For example, $k = 1.0$, Z'_{IM} yields $\omega^+ = 2.0409 - i0.8801$ and $\omega^- = -0.4542 + i3.5173E-5$; Z'_{IM0} yields $\omega = 2.0843 - i0.7871$, whereas IVP simulation yields $\omega \simeq 0.454 + i0$. Our solutions of ω^\pm via GPDF are in favor of the solutions by Baalrud.⁵ This benchmark provides further verification of the one-solve-all scheme.

Fig. 13 shows that the discontinuity point at $v = \nu$ changes the dispersion properties considerably, for instance,

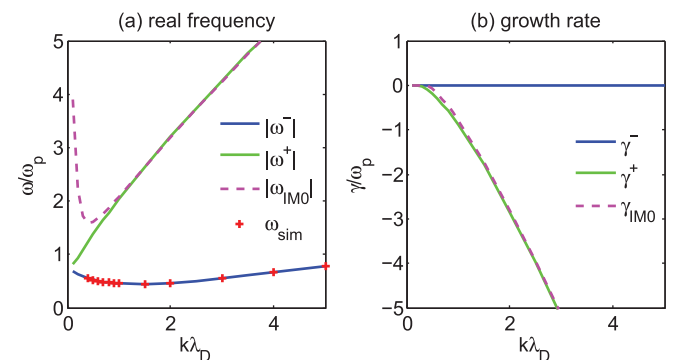


FIG. 13. Dispersion relation solutions (root finding) of incomplete Maxwellian distribution with $\nu = -0.1v_t$, which agree with the simulation results very well.

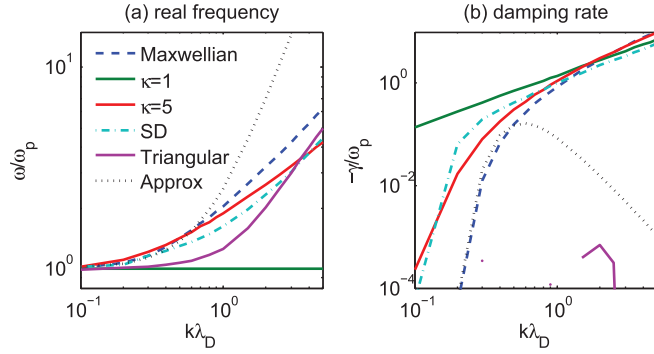


FIG. 14. Distribution function effects on Landau damping with different initial distributions, where the approximate solution by Eq. (33) for Maxwellian distribution is also shown.

a new nearly undamped branch can be found, which should be caused by the lack of resonance particles at $v_p = \omega/k < v$. The differences between the solutions of $Z'_{IM}(\zeta)$ and $Z'_{IM0}(\zeta)$ also indicates that an incorrect treatment of discontinuity point will yield inaccurate results.

C. Results of distribution function effects

We use GPDF to revisit the distribution function effects on Landau damping.

For Maxwellian distribution and small k , approximate analytical expressions for real frequency and growth rate are¹

$$\omega_r^2 = \omega_p^2(1 + 3k^2\lambda_D^2), \quad (33a)$$

$$\omega_i = \frac{\pi \omega_r^3}{2 k^2} \frac{\partial f_0}{\partial v} \bigg|_{v=\omega_r/k}. \quad (33b)$$

The effects of κ -distribution on Landau damping, particularly for space plasma, are discussed in detail by Thorne and Summers.¹³ The incomplete Maxwellian distribution is discussed by Baalrud.⁵

We choose Maxwellian, κ , and slowing down distributions with $v_t = \sqrt{2}$ as well as triangular distributions with the same parameters as in Fig. 9 for further comparisons. Fig. 14 shows the results of ω_r vs. k and γ vs. k . For triangular distribution, a non-zero γ around $\pm 10^{-4}$ exists but is sensitive to initial guessing for the root finding, which should be caused by the jump of Z' around $\Im(z) = 0$ as shown in Fig. 9.

Table I shows the quantitative value of the solutions, where ω^G is solved from GPDF and ω^S is from IVP simulation. For non-smooth input distributions, the simulation is not robust and is sensitive to parameters and initial conditions. Several results in table ($k = 1.0$) are very rough (labeled with ‘ \simeq ’). For instance, the error of the result in this table for slowing down distribution is very large (approximately 10%), whereas, for small k and small damping rate, e. g., $k = 0.5$, IVP simulation is more robust and accurate, and we obtain $\omega_{SD}^S = 1.29 - 0.42i$ compared with $\omega_{SD}^G = 1.2876 - 0.4119i$.

TABLE I. Comparison of the Langmuir wave solutions with different distribution functions and $k = 1.0$.

	ω_r^G	ω_i^G	ω_r^S	ω_i^S
Maxwellian	2.0459	-0.8513	2.01	-0.85
$\kappa = 1$	1.0000	-1.4142	1.00	-1.40
$\kappa = 5$	1.8786	-1.0866	1.82	-1.08
Slowing down	1.6240	-0.9975	$\simeq 1.68$	$\simeq -0.87$
Triangular	1.2577	4.2×10^{-4}	$\simeq 1.26$	$\simeq 0.005$

V. SUMMARY AND DISCUSSION

The analytical properties and one-solve-all numerical scheme for generalized plasma dispersion function, which provides a useful tool for treating linear effects of almost arbitrary distribution functions, are discussed. The exact distribution function effects on Landau damping are revisited to demonstrate an application.

The one-solve-all scheme can also be used analytically as an expansion method for GPDF, in addition to the usual Taylor expansion scheme used.

Our method cannot be used directly for relativistic^{14,15} or other more complicated dispersion functions because those dispersion functions are usually not in HT form. However, similar orthogonal functions expansion treatment may be used, as mentioned by Robinson.⁷

ACKNOWLEDGMENTS

Discussions with Y. R. Lin-Liu at the early stage of this project to understand the treatment of usual PDF are appreciated. This work is support by the NSF of China under Grant No. 11235009, the ITER-CN under Grant No. 2013GB104004 and Fundamental Research Fund for Chinese Central Universities.

¹D. R. Nicholson, *Introduction to Plasma Theory* (Wiley, 1983).

²B. D. Fried and S. D. Conte, *The Plasma Dispersion Function the Hilbert Transform of the Gaussian* (Academic Press, New York and London, 1961); “Erratum,” *Math. Comput.* **26**(119), 814 (1972), see <http://www.ams.org/journals/mcom/1972-26-119/S0025-5718-1972-0655816-4/>; “Reviews and descriptions of tables and books,” *Math. Comput.* **17**, 94–95 (1963), see <http://www.ams.org/journals/mcom/1963-17-081/S0025-5718-1963-1781088-8/>.

³F. Valentini and R. D’Agosta, *Phys. Plasmas* **14**, 092111 (2007).

⁴D. Summers and R. M. Thorne, *Phys. Fluids B* **3**, 1835 (1991).

⁵S. D. Baalrud, *Phys. Plasmas* **20**, 012118 (2013).

⁶M. A. Hellberg and R. L. Mace, *Phys. Plasmas* **9**, 1495 (2002).

⁷P. A. Robinson, *J. Comput. Phys.* **88**, 381 (1990).

⁸J. A. C. Weideman, *Math. Comput.* **64**, 745 (1995).

⁹J. A. C. Weideman, *SIAM J. Numer. Anal.* **31**, 1497 (1994).

¹⁰W. D. Jones, H. J. Doucet, and J. M. Buzzi, *An Introduction to the Linear Theories and Methods of Electrostatic Waves in Plasmas* (Springer, 1985).

¹¹P. Guio, J. Liliensten, W. Kofman, and N. Bjorna, *Ann. Geophys.* **16**, 1226 (1998).

¹²H. S. Xie, “Constant residual electrostatic electron plasma mode in Vlasov-Ampere system,” *Phys. Plasmas* (submitted).

¹³R. M. Thorne and D. Summers, *Phys. Fluids B* **3**, 2117 (1991).

¹⁴B. B. Godfrey, B. S. Newberger, and K. A. Taggart, *IEEE Trans. Plasma Sci.* **3**, 60 (1975).

¹⁵F. Castejon and S. S. Pavlov, *Phys. Plasmas* **13**, 072105 (2006).

¹⁶See supplementary material at <http://dx.doi.org/10.1063/1.4822332> for the MATLAB version numerical routines, where GPDF, root finding, IVP simulation and test plotting codes are included.